Geoscience Frontiers 11 (2020) 1609–1620

HOSTED BY

Contents lists available at ScienceDirect

Geoscience Frontiers

journal homepage: www.elsevier.com/locate/gsf

Research Paper

Comparison of machine learning models for gully erosion susceptibility mapping

Alireza Arabameri [a], Wei Chen [b,c,d], Marco Loche [e], Xia Zhao [b], Yang Li [b], Luigi Lombardo [f], Artemi Cerda [g], Biswajeet Pradhan [h,i,*], Dieu Tien Bui [j]

[a] Department of Geomorphology, Tarbiat Modares University, Tehran, Iran
[b] College of Geology & Environment, Xi'an University of Science and Technology, Xi'an 710054, China
[c] Key Laboratory of Coal Resources Exploration and Comprehensive Utilization, Ministry of Land and Resources, Xi'an 710021, China
[d] Shaanxi Provincial Key Laboratory of Geological Support for Coal Green Exploitation, Xi'an 710054, China
[e] Università Degli Studi di Cagliari, Dipartimento di Scienze Chimiche e Geologiche, 09042, Monserrato, Cagliari, Italy
[f] University of Twente, Faculty of Geo-Information Science and Earth Observation (ITC), PO Box 217, Enschede, AE 7500, Netherlands
[g] Soil Erosion and Degradation Research Group, Departament de Geografia, Universitat de València, Blasco Ibàñez, 28, 46010, Valencia, Spain
[h] Centre for Advanced Modelling and Geospatial Information Systems (CAMGIS), Faculty of Engineering and Information Technology, University of Technology Sydney, New South Wales, Australia
[i] Department of Energy and Mineral Resources Engineering, Sejong University, Choongmu-gwan, 209 Neungdong-ro Gwangjin-gu, Seoul, 05006, Republic of Korea
[j] Institute of Research and Development, Duy Tan University, Da Nang, 550000, Viet Nam

ARTICLE INFO

Handling Editor: M. Santosh

Keywords:
Oil erosion
GIS
Alternating decision tree model
Logistic model tree model

ABSTRACT

Gully erosion is a disruptive phenomenon which extensively affects the Iranian territory, especially in the Northern provinces. A number of studies have been recently undertaken to study this process and to predict it over space and ultimately, in a broader national effort, to limit its negative effects on local communities. We focused on the Bastam watershed where 9.3% of its surface is currently affected by gullying. Machine learning algorithms are currently under the magnifying glass across the geomorphological community for their high predictive ability. However, unlike the bivariate statistical models, their structure does not provide intuitive and quantifiable measures of environmental preconditioning factors. To cope with such weakness, we interpret preconditioning causes on the basis of a bivariate approach namely, Index of Entropy. And, we performed the susceptibility mapping procedure by testing three extensions of a decision tree model namely, Alternating Decision Tree (ADTree), Naïve-Bayes tree (NBTree), and Logistic Model Tree (LMT). We dichotomized the gully information over space into gully presence/absence conditions, which we further explored in their calibration and validation stages. Being the presence/absence information and associated factors identical, the resulting differences are only due to the algorithmic structures of the three models we chose. Such differences are not significant in terms of performances; in fact, the three models produce outstanding predictive AUC measures (ADTree = 0.922; NBTree = 0.939; LMT = 0.944). However, the associated mapping results depict very different patterns where only the LMT is associated with reasonable susceptibility patterns. This is a strong indication of what model combines best performance and mapping for any natural hazard – oriented application.

1. Introduction

Soil erosion is by far one of the primary natural hazard which may threaten communities at the societal scale (Amundson et al., 2015; Dazzi et al., 2019; Herrick et al., 2019). Overall, 99.7% of our food originates from the soil, and the remaining 0.03% is sourced from marine ecosystems (Pimentel and Burgess, 2013). And, looking at how soil erosion is globally distributed, Asia is the most subjected continent with 35 million hectares removed each year, followed by Africa, America and Europe (Cartagena, 2004; Panagos et al., 2015). Thus, adopting sustainable practices for soil conservation is a mandatory requirement to sustain lives in the future (Kümmerer et al., 2010). Soil erosion can be

* Corresponding author. Centre for Advanced Modelling and Geospatial Information Systems (CAMGIS), Faculty of Engineering and Information Technology, University of Technology Sydney, New South Wales, Australia.
E-mail addresses: Biswajeet.Pradhan@uts.edu.au, biswajeet24@gmail.com (B. Pradhan), buitiendieu@gmail.com (D.T. Bui).
Peer-review under responsibility of China University of Geosciences (Beijing).

https://doi.org/10.1016/j.gsf.2019.11.009
Received 3 August 2019; Received in revised form 24 October 2019; Accepted 16 November 2019
Available online 6 December 2019

promoted by several processes: (1) anthropogenic, such as agricultural practices (Zhao and Hou, 2019) and deforestation (Gholami, 2013); or (2) natural, such as overland water flows (Xiong et al., 2018) and wind (Skidmore, 1982).

Iran is a country where soil erosion occurs at a very fast rate making it a national threat to be addressed. The literature reports a mean yearly rate of 1500 tons/km^2 permanently washed away which translates into 1 mm/yr reduction in soil thickness across the whole Iranian surface (REFAHI, 2009). These values are due to the specific geographic setting in Iran, where the climate is arid to semi-arid and 75.8% of the national territory is exposed to water erosion (REFAHI, 2009). This combination leads to prolonged dry seasons and short wet periods, during which large amounts of precipitation are discharged, promoting runoff over infiltration processes.

Among the natural or primarily natural processes which influence soil erosion, water represents the main driver; and, among water-driven erosion types, gully erosion is particularly devastating because it is able to quickly remove and transport large volumes of soil. Numerous examples are shown in the literature where several meters of incisions extend over the vertical direction and hundreds meters may extend over the horizontal direction (e.g., Daba et al., 2003; Imwangana et al., 2014; Kropacek et al., 2016). And, Iran has been reported to host some of the most daunting gully incisions across the globe (Arabameri et al., 2018d, 2019b,c). This is the main reason behind the recent national effort in Iran to understand erosion patterns (Arabameri et al., 2018a, b) because for such a large country, prioritizing investments and planning conservation practices are very complex tasks. Thus, prior to any action, the main research institutions in Iran have been tasked to map the spatial tendency or the susceptibility to gully. This information will serve as the base to recognize gully "hotspots" from current and predicted data of the gullying process.

Contrary to other water-driven natural hazards where physically based models can produce a reliable representation of the space-time evolution of a given process such as floods (Roux et al., 2011; Arabameri et al., 2019f), debris flows (Bout et al., 2018) and widespread soil erosion, gully erosion susceptibility models are primarily built via statistical or machine learning tools (Akgün and Türk, 2011; Conforti et al., 2011). Among these, a wide range of methods have been tested in the literature, spanning from simple bivariate models (Rahmati et al., 2016) to more appropriate multivariate models in their parametric (e.g. Logistic Regression; Lucà et al., 2011) and non-parametric equivalents (e.g. Boosted Regression Tree; Rahmati et al., 2017). Each of these methods has found its niche for different reasons. Bivariate models are well integrated within the Geographic Information System (GIS) environment, for the equations upon which they rely can be easily solved in GIS via basic packages, and because of their simple interpretation (Magliulo, 2012). However, they do not rely on a specific probability distribution, thus making the susceptibility estimates the result of ad-hoc procedures (Lombardo and Mai, 2018). This is not the case for parametric statistical models such as Generalized Linear Models (GLM; Gutiérrez et al., 2010), where gully phenomena are assumed to be spread over space according to a Bernoulli probability distribution (Lombardo et al., 2016a; Lombardo and Mai, 2018). As a result, the derived susceptibility maps are objective and comparable. However, the calculations cannot be entirely implemented within GIS. In fact, once the pre-processing phase is complete, then one needs to run these algorithms in a computing environment (e.g. R, Python or Matlab) and re-import back the results into GIS. However, in the vast majority of studies, the geomorphological use of multivariate statistical approaches results in maps that are quite smooth over space (e.g., Lombardo et al., 2015, 2019a; Pourghasemi and Rossi, 2017). This is not the case for non-parametric machine learning models (e.g. Decision Trees and their variations) (Kheir et al., 2008) where each predictor is repeatedly dissected as the tree grows resulting in extremely detailed susceptibility maps and associated high performances (sometimes affected by overfit) (Dietterich, 1995).

Considering such differences, the current scientific trend combines their strengths, keeping the simple interpretability of a bivariate structure while exploiting the predictive capacity of the machine learning algorithms. This is the case in the present study, where we aligned our scientific interest in this current trend. Specifically, we adopted Index of Entropy (Pourghasemi et al., 2012) to interpret the effect of conditioning factors on gully occurrences whereas for mapping, we tested three different methods namely, Alternating Decision Tree (ADTree) (Chen et al., 2017b), Naïve-Bayes tree (NBTree) (Tien Bui et al., 2012), and Logistic Model Tree (LMT) (Arabameri et al., 2018a).

The main rationale of our work is to check whether the three machine learning approaches produce satisfactory performances which could be implemented in the Iranian context for gully erosion susceptibility mapping, and more generally in other areas exposed to the same threat. In this workflow, we also include state-of-the-art GIS and Remote Sensing applications. We derived the morphometric properties from one of the ALOSPALSAR DEM with a spatial resolution of 12.5 m (Niipele and Chen, 2019). And, we also used NDVI as a proxy for the Land Use/Cover within the study area through LANDSAT 8 images with 30 m spatial resolution. Notably, the data used in this work is the same collected and reported in Arabameri et al. (2019h), where the same data was processed via ensemble models.

The paper is organized as follows: Section 2 summarized the study area; Section 3 describes the model, thus reporting the information on the gullies (target variable), environmental factors (explanatory variables) and model structure; Section 4 reports the model results which are further interpreted in Section 5; Sections 6 provides concluding remarks, how the present research fits into the current literature and how it can be useful for future studies.

2. Study area

The Bastam watershed covers roughly 1329 km^2 area (36°27′02″ to 36°47′13″N, and 54°24′23″ to 55°11′08″E; Fig. 1). Elevation ranges from 1357 m. a.s.l. to 3893 m. a.s.l., with a mean of 2783 m. a.s.l. Because this variation is contained in a relatively small surface, the associated steepness can locally reach quite significant values, these being bounded between 0° and 71° with a mean of 14°. However, their distribution is not uniform for the central and southern sectors of the watershed exhibit a relatively smooth topography with gentle slopes. The rest of the study area is mountainous, being part of the Alborz Mountains. The watershed is subjected to a mean annual rainfall of 262 mm, which follows a heterogeneous pattern between dry and wet seasons. A similar trend affects the local temperatures with a yearly mean of 13 °C (IRIMO, 2012). More than 25% of the land is poor rangeland. Another 22.84% is covered by a relatively sparse forest, while 0.01% is covered in dense forest and 0.01% is land for dryland-farming. The main lithographic units consist of high elevation piedmont fans and valley terrace deposits, stream channels, braided channels, floodplain deposits, and low elevation piedmont fans, and valley terrace deposits (GSI, 1997). Rock outcrops, entisols, entisols/inceptisols, and mollisols are the most common geological and pedological materials in the study area. Approximately 9.3% of the study area is affected by gully erosion (GSI, 1997). However, the gully distribution is also heterogeneous; there are more gullies in the southern-central portion of the study area where slopes are gentle. Conversely, no gullies develop in the northern sector where slopes are steep and rocky outcrops are abundant. Gullies range in length from several meters to several hundred meters, and their vertical incisions are generally several meters deep. Gully width also varies, ranging from several centimeters to several meters. Such morphometric variability results in a differentiation in the resulting landforms. In fact, gullies developed in the northern parts of the study area have V-shaped cross-sections, whereas in the central and southern parts of the region, due to more erodible soils, concentrated runoff (due to a gentler slope) and more resistant sediments, they are primarily U-shaped.

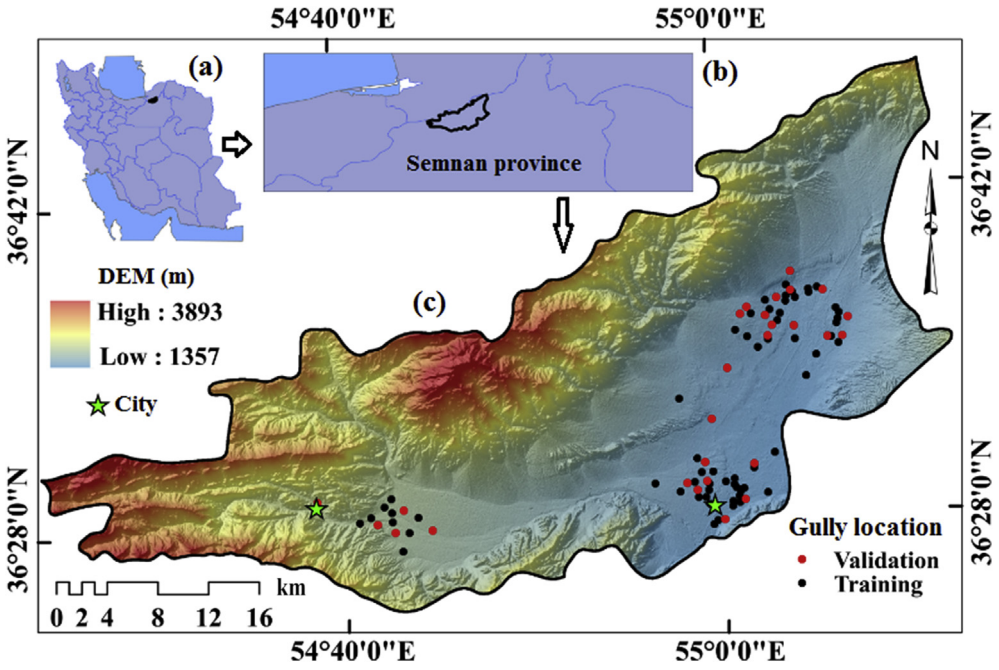

Fig. 1. Study area. (a) Location of Semnan province and study area in Iran, (b) location of study area in Semnan province, (c) location of training and validation dataset in study area. Figure modified from Arabameri et al. (2019).

3. Material and methods

3.1. Gully erosion inventory map

The Gully Erosion Inventory Map (GEIM) reports the locations where gullies have been mapped and represents the information upon which any predictive model is trained to explain the spatial distribution of susceptible conditions to gullying (Arabameri et al., 2018d). We initially acquired the GEIM from the Agricultural and Natural Resources Research Center of Semnan Province and subsequently validated the reported locations through extensive field surveys using Global Position System and interpretation of high-resolution images collated from Google Earth on June 11, 2015 (WorldView-2, spatial resolution of 0.5 m) and November 11, 2016 (from Pleiades-1, spatial resolution of 0.5 m). Overall, 303 gullies were identified and mapped in the study area (Fig. 1). Their maximum and minimum lengths are 346 m and 0.74 m, respectively. As for the vertical incision, the maximum depth is 7.2 m and the minimum depth is 0.65 m; this is associated with a maximum width of 16.6 m and a minimum width of 0.74 m. From the mapped gullies we extracted the head-cuts to represent the location where the process primarily starts and develops over time (Hosseinalizadeh et al., 2019a). To prepare the dataset for the modeling phase, we randomly split the head-cut distribution into a calibration (70% or 212 gullies) and validation (30% or 91 gullies) sets. Each set is merged together with an equal number of random locations expressing the absence of the gulling process over space (Camilo et al., 2017). We created the absence subsets by using the random-point tool in ArcGIS and ultimately built a balanced dataset of gully presences-absences (Lombardo et al., 2014). This is a common procedure in gully erosion susceptibility as well as for many other natural hazards (Nefeslioglu et al., 2008; Pourghasemi et al., 2017) which is used to create two balanced sets which represent the target variable that our models take on to construct the susceptibility maps (Arabameri et al., 2018c, 2019a; Zabihi et al., 2018).

3.2. Environmental factors

Choosing informative conditioning factors is crucial to find functional relationships with gully occurrences that would lead to satisfying performance (Rahmati et al., 2016). Gullying occurs globally but local geographic conditions can promote the role of different conditioning factors (Arabameri et al., 2019i). Nevertheless, it is quite customary to adopt geo-environmental factors that would carry the signal of topography, hydrology, climatology, soil characteristics, land use/land cover and human kind activities (Montgomery and Dietrich, 1992; Poesen et al., 1998; Kheir et al., 2007; Takken et al., 2008; Samani et al., 2009; Capra et al., 2012; Parras-Alcántara et al., 2016; Arabameri et al., 2019i). Here we chose eighteen factors (Fig. 2a–r) in accordance to the literature suggestion (Montgomery and Dietrich, 1992; Poesen et al., 1998; Kheir et al., 2007; Takken et al., 2008; Samani et al., 2009; Capra et al., 2012; Parras-Alcántara et al., 2016; Arabameri et al., 2019i). Moreover, we made expert choices on the basis of data availability for Semnan and Isfahan provinces. By testing for multicollinearity no conclusive estimation pointed out for the exclusion of the factor we originally selected. The source data used to derive the conditioning factors is listed below: ALOS DEM at 12.5 m, LANDSAT 8 at 30 m, Meteorology data, as well as topographic and thematic maps locally available thanks to different Iranian institutions working on natural resources.

Eleven conditioning factors represent the morphometric settings of the area, encompassing: (1) Slope angle (Zevenbergen and Thorne, 1987) (Fig. 2a); (2) Aspect (Zevenbergen and Thorne, 1987) (Fig. 2b); (3) Elevation (Fig. 2c); (4) Plan curvature (Fig. 2d); (5) Profile curvatures (Heerdegen and Beran, 1982) (Fig. 2e); (6) Convergence index (Olaya and Conrad, 2009) (Fig. 2f); (7) LS Factor (Desmet and Govers, 1996) (Fig. 2g); (8) Terrain ruggedness index-TRI (Fig. 2h); (9) Topographic position index (Reu et al., 2013) (Fig. 2i); (10) Stream power index (Moore and Grayson, 1991) (Fig. 2j); and (11) Topographic wetness index – TWI (Beven and Kirkby, 1979) (Fig. 2k). We complement this information with three proxies of hydrological properties, these being: (12) Rainfall (Fig. 2m); (13) Drainage density (Arabameri et al., 2018c) (Fig. 2n); (14) Distance to streams (Trigila et al., 2015) (Fig. 2o). We also considered the factors associated with anthropogenic influences on the environment namely, (15) Distance to road (road network being extracted from the local topographic map at 1:50,000) (Fig. 2l) and (16) Land Use/Cover (obtained by classifying the Normalized Difference Vegetation Index obtained from LANDSAT 8 scenes) (Fig. 2q). To finalize our selected predictor set, we included the outcropping lithology

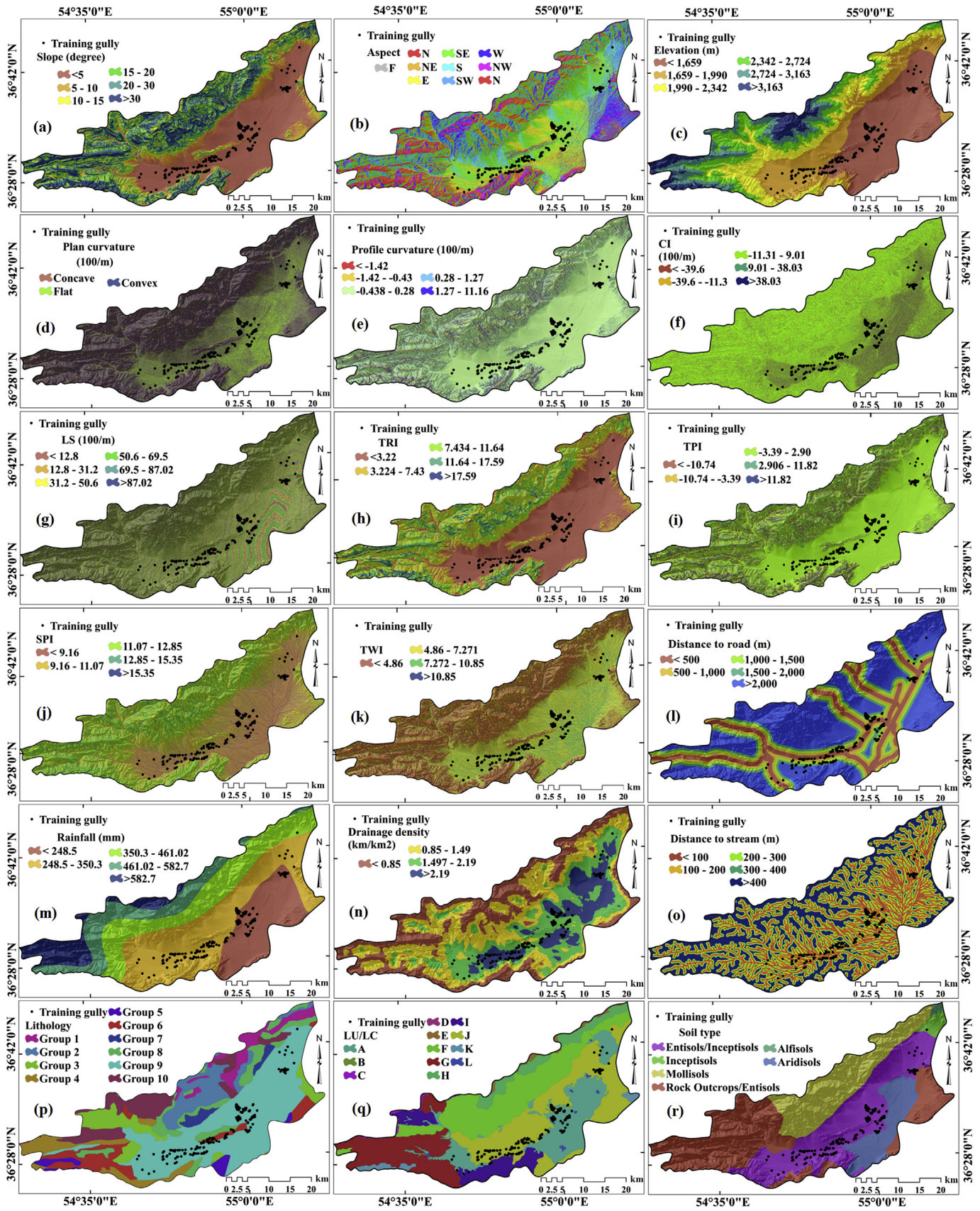

Fig. 2. Gully erosion conditioning factors. (a) Slope, (b) aspect, (c) elevation, (d) plan curvature, (e) profile curvature, (f) convergence index (CI), (g) slope length (LS), (h) terrain ruggedness index (TRI), (i) topography position index (TPI), (j) stream power index (SPI), (k) topography wetness index (TWI), (l) distance to road, (m) rainfall, (n) drainage density, (o) distance to stream, (p) lithology, (q) land use/land cover (LU/LC), and (r) soil type.

(obtained from the local geological map at 1:100,000-scale) (GSI, 1997) (Fig. 2p) and soil types (provided by the Semnan Agricultural and Natural Resources Research Centre) (Fig. 2r). Description of lithology units in the study area are shown in Table 1. Details of thematic layer preparation and extraction are explained in Arabameri et al. (2018c, 2019a, 2019h) and Rahmati et al. (2019).

More specifically, we opted to include elevation as it influences vegetation and precipitation as well as gully erosion occurrences, as also reported by Golestani et al. (2014). We opted to reclassify it in six classes: <1659 m, 1659–1990 m, 1990–2342 m, 2342–2724 m, 2724–3163 m and >3163 m (Fig. 2c).

Similarly, slope water runoff and the drainage network and its influence on gullying has been reported in several studies (e.g., Ghorbani Nejad et al., 2016). We represented slope into six classes <5, 5–10, 10–15, 15–20, 20–30, and >30 (Fig. 2b).

Aspect controls the solar radiation exposure and therefore soil moisture and evapotranspiration regimes. Its use as a conditioning factor is common across gully erosion susceptibility studies (e.g., Jaafari et al., 2014) and we chose to classify it into nine classes: flat, N, NE, E, SE, S, SW, W and NW (Fig. 2a).

Planar curvature controls convergence and divergence of downslope water fluxes and its role in the gully erosion studies has several examples (Golestani et al., 2014). We chose to reclassify it into three classes to represent concave, flat and convex conditions (Fig. 2d).

The topographic wetness index indicates the tendency of a given location to receive overland flows as a function of the upslope contributing area and therefore could provide information on gully formation and evolution (Golestani et al., 2014). We represented this factor by classifying it into four classes <4.86, 4.86–7.27, 7.27–10.85 and > 10.85 (Fig. 2k).

The CI, TRI, SPI and TPI are four factors known to represent the morphology of the terrain and the influence that this may have on water flows (Claps et al., 1994) which we represented into five classes for the CI and four classes for the remaining cases.

To additionally take into consideration hydrology and human influences we computed distances from rivers and roads according to Zakerinejad and Maerker (2015) as well as drainage density (Golestani et al., 2014).

We also brought into the model the lithological control on gullying by using lithological units (Golestani et al., 2014). Ultimately, we used Land use/Land cover to carry the overall signal that the contrast between bare lands and vegetated ones have on gully erosion (Zakerinejad and Maerker, 2015).

Table 1
Lithology of the study area.

Group	Description
1	Limestone with subordinate black shale
2	Yellowish, thin to thick-bedded, fossileferous argillaceous limestone, dark grey limestone, greenish marl and shale, locally including gypsum
3	Andesitic to basaltic volcanosediment, well bedded green tuff and tuffaceous shale, andesitic and basaltic volcanics
4	Light grey, thin-bedded to massive limestone, well-bedded to thin-bedded, greenish-grey argillaceous limestone with intercalations of calcareous shale
5	Upper Cretaceous, undifferentiated rocks marl, shale and detritic limestone
6	Red conglomerate and sandstone, gypsiferous marl, red conglomerate and sandstone
7	Greenish-grey siltstone and shale with intercalations of flaggy limestone
8	Red sandstone and shale with subordinate sandy limestone, polymictic conglomerate and sandstone, andesitic basaltic volcanic, undifferentiated Permian rocks; Reef-type limestone and gypsiferous marl, fluvial conglomerate, piedmont conglomerate and sandstone
9	High level piedmont fan and vally terrace deposits, stream channel, braided channel and flood plain deposite, low level piedment fan and vally terrace deposits
10	Thick bedded dolomite, dark grey shale and sandstone

Due to the large predictor hyperspace we have built, potential multicollinearity issues may arise during the modeling stages. Linear models tend to suffer from multicollinearity much more than machine learning ones, although it is always preferable to eliminate redundant information. For this reason, we have run the multicollinearity assessment prior to any analyses, and the results are reported in the following section.

Ultimately, because we decided to interpret the relations between conditioning factors and gully occurrences using the IoE (a bivariate model), we had to reclassify each continuous conditioning factor into a finite set of subclasses to calculate the proportion of gully-no gully data in each class (Arabameri et al., 2018c, 2019a).

3.3. Multicollinearity assessment

We tested for multicollinearity by using the Variance Inflation Factor (VIF, see details in Cama et al. (2017)) and Tolerance (see details in Arabameri et al. (2018c)) metrics. The former indicates linear relationships among conditioning factors when VIF ≥10 whereas the latter confirms the same hypothesis for Tolerance ≤0.1. The result of the collinearity analysis is reported in Table 2 where no cases exceed the thresholds for multicollinearity. Since no collinear conditioning factors were found, we proceeded to slice the continuous factors reported in Table 2. This is a pre-requirement for the subsequent modeling phases. It should be noted that multicollinearity in the linear domain is routinely checked in any statistical application although it does not guarantee that multicollinearity will not appear after binning the continuous conditioning factors into classes. However, detecting multicollinearity for such cases is still a matter of debate even in the statistical community and thus we chose to proceed assuming that no linear dependency among conditioning factors would negatively affect our susceptibility models (Kelava et al., 2008).

3.4. Model structure

3.4.1. Index of entropy

The Index of Entropy (IoE) method finds its theoretical foundation in Thermodynamics and Information Theory. In natural hazards it has proven to be useful to determine causal effects of environmental properties over a certain process distributed over space (Lombardo et al., 2016b). The equations to be solved to compute the IoE are provided in (Jaafari et al., 2014) and the descriptive explanation of the model is given below.

The approach can only take on conditioning factors that are categorical in nature. Thus, from original continuous properties, the first step is to reclassify each predictor into a number of classes. For each predictor (j) and associated classes (i), the proportion (Pr) of gully presence can be calculated as the ratio between the number of gullies (n_i) falling in a given class and the number of pixels (m_i) representing that class. The relation ($Pr_{ij} = n_i/m_i$) is then converted into a density (Pd_{ij}) by dividing each proportion Pr_{ij} by the sum of all the proportions associated with a specific factor. These densities serve as a reference to compute two entropy indices (H_j and H_{jmax}). H_j is obtained as the opposite of the sum of

Table 2
Multi-collinearity test among gully erosion conditioning factors.

Factors	Collinearity Statistics		Factors	Collinearity Statistics	
	Tolerance	VIF		Tolerance	VIF
Drainage density	0.322	3.107	Rainfall	0.289	4.179
Distance to road	0.685	1.460	Lithology	0.271	3.688
Slope	0.543	1.498	Soil type	0.471	2.124
Plan curvature	0.494	2.025	TWI	0.374	3.509
Profile curvature	0.508	1.968	SPI	0.584	1.919
Distance to stream	0.604	1.655	TPI	0.392	2.553
LS	0.975	1.025	LU	0.265	3.778
Aspect	0.902	1.109	Elevation	0.643	1.276
CI	0.635	1.574	TRI	0.426	2.265

all densities for a given factor multiplied by the binary logarithm of each density. H_{jmax} is just the binary logarithm of the total number of classes for each factor.

These are the preparatory steps in order to finalize the Index of Entropy model and extract the weights which we will use for the interpretation. In fact, the so-called Information Coefficient (IC_j) is calculated for each class as the normalized ratio between the entropy indices: $IC_j = (H_{jmax} - H_j)/H_{jmax}$ and, the final weights (W_j) for each class are simply the product between the Information Coefficients (IC_j) and the initial proportions (Pr_{ij}). A susceptibility map can also be produced by summing the weights associated with the spatial bins of each conditioning factor.

3.4.2. Alternating decision tree

Alternating decision tree (ADTree) is the combination of decision tree and boosting algorithm, and proposed by (Freund and Mason, 1999). The ADTree model has higher accuracy than standard model trees in classification problems (Sok et al., 2016). In generally, ADTree model consists of two kinds of nodes: splitter node and prediction node. The splitter node divides the data based on selected attribute values and prediction node includes the numerical score which used to make the prediction (Pham et al., 2017). A basic ruler that maps from instances to real numbers consists of a prediction c_1, a base condition c_2 and two real numbers: a and b. The prediction is a when $c_1 \cap c_2$ or b when $c_1 \cap^{-} c_2$. The values of a and b is calculated by the following equations.

$$a = \frac{1}{2}\ln\frac{W_+(c_1 \cap c_2)}{W_-(c_1 \cap c_2)} \tag{1}$$

$$b = \frac{1}{2}\ln\frac{W_+(c_1 \cap^{-} c_2)}{W_-(c_1 \cap^{-} c_2)} \tag{2}$$

where the best c_1 and c_2 are selected by the minimizing the $Z_t(c_1, c_2)$ and is defined as:

$$Z_t(c_1, c_2) = 2\sqrt{W_+(c_1 \cap c_2)W_-(c_1 \cap c_2)} + \sqrt{W_+(c_1 \cap^{-} c_2)W_-(c_1 \cap^{-} c_2)} + W(\overset{\bullet}{\bullet} c_2) \tag{3}$$

Suppose M is the set base rules, then a new rule can be defined as $M_t{+}1{=}M_t + r_t$. $r_t(x)$ shows the two prediction values (a and b) at each later of the tree and x is a set of instances. The classification can be regarded as the sign of accumulation of prediction values in $M_t{+}1$.

$$\mathrm{Class}(x) = \mathrm{sign}\left(\sum_{t=1}^{T} r_t(x)\right) \tag{4}$$

3.4.3. Naïve-Bayes tree

Naive Bayes tree (NBTree) is an ensemble model that consists of Naive Bayes (NB) and decision tree (Huang et al., 2003; Wang et al., 2015). Roughly, it can be considered a naive Bayes classifier is applied to each leaf node when the decision tree is constructed (Chen et al., 2017a). The NBTree is a commonly used machine learning algorithm which has been used by many scholars in landslide susceptibility assessment and achieved satisfactory performance (Chen et al., 2017a; Pham et al., 2017). The classification rule of NB can be expressed as follows:

$$c^{*} = \mathrm{arcmax}_{c_j \in C}\ P(c_j|a_1,\ a_2,\ \ldots,\ a_m) = \frac{P(c_j)\prod_{i=1}^{m} p(a_i|c_j)}{\sum_{j=1}^{k}[p(c_j)\prod_{i=1}^{m} p(a_i|c_j)]} = \mu\mathrm{arcmax}_{c_j \in C} P(c_j)\prod_{i=1}^{m} P(a_i|c_j) \tag{5}$$

where c_j is the class attribute of class set C. a_1, a_2, …, a_m are the conditionally independent and k is the total number of classes.

3.4.4. Logistic model tree

Logistic model tree (LMT), proposed by Landwehr (2003), is a classification algorithm based on decision tree and logical regression. The model uses LogitBoost algorithm to establish the logistic regression function on the nodes of the tree and CART algorithm for pruning (Chen et al., 2019). The model applies cross-validation to find multiple LogitBoost iterations to prevent overfitting of training data (Tien Bui et al., 2016). The LogitBoost model introduces least squares fitting additive logistic regression for each M_i class and the posterior probability of leaf nodes is calculated by linear logistic regression (Wang et al., 2016; Kadavi et al., 2019).

$$L_M(x) = \sum_{i=1}^{n} \beta_i x_i + \beta_0 \tag{6}$$

$$P(M|x) = \frac{\exp(L_M(x))}{\sum_{M'=1}^{D} \exp(L_M{}'(x))} \tag{7}$$

where β_i is the coefficient of the ith component of vector x, n is the number of factors and D is the number of classes.

3.5. Model validation

We base our model validation upon Receiver Operating Characteristic (ROC) curves and associated integrals namely Area Under the Curve (Arabameri et al., 2019d, e, f). The ROC is a common cut-off-independent diagnostic which can be obtained for any two vectors (Mandrekar, 2010; Rahmati et al., 2019), where the first one expresses the binary condition of presence-absence of a given process and the second vector reports the corresponding probability estimates (Chen et al., 2019; Lombardo et al., 2019b). According to the classification proposed by Hosmer and Lemeshow (2000), the overall model performance can be recognized as a function of AUC values. Specifically, AUC = 0.5 corresponds to a purely random guess; then, as the AUC increases towards ideal predictions (AUC = 1.0), three main performance classes have been proposed: 0.7 < AUC < 0.8 is considered acceptable, 0.8 < AUC < 0.9 is considered excellent, and AUC > 0.9 is considered outstanding (Hosmer and Lemeshow, 2000).

3.6. Summary of methodology

Based on the above theories, this study consists of several main stages which we describe here and summarize in Fig. 3: (i) Data Preparation, which includes selection and preparation of gully erosion conditioning factors (GECFs) and gully erosion inventory map (GEIM); (ii) Multicollinearity analysis (MA) using tolerance (TOL) and variance inflation factor (VIF) according to Cama et al. (2017); (iii) determine the spatial relationship between GECFs and gully locations using the Index of Entropy model; (iv) gully erosion susceptibility mapping using ADTree, NBTree and LMT; (v) validation through AUC.

4. Results

This section reports the results from an interpretative standpoint of predictors' effects and in terms of predictive performance.

4.1. Conditioning factors' effect using index of entropy model

Table 3 reports the weights coming from the IoE method. Slope, Rainfall and Drainage Density show the greatest degree of influence with respect to gully occurrences. This is particularly interesting for the IoE highlights factors which are linked to hydrological conditions which is the primary cause of gullies from an expert-based perspective. Specifically, Slope has an overall weight of 0.48, whereas Rainfall and Drainage Density are associated with weights equal to 0.448 and 0.565. In turn, this implies that drainage plays the most relevant role and, in conjunction

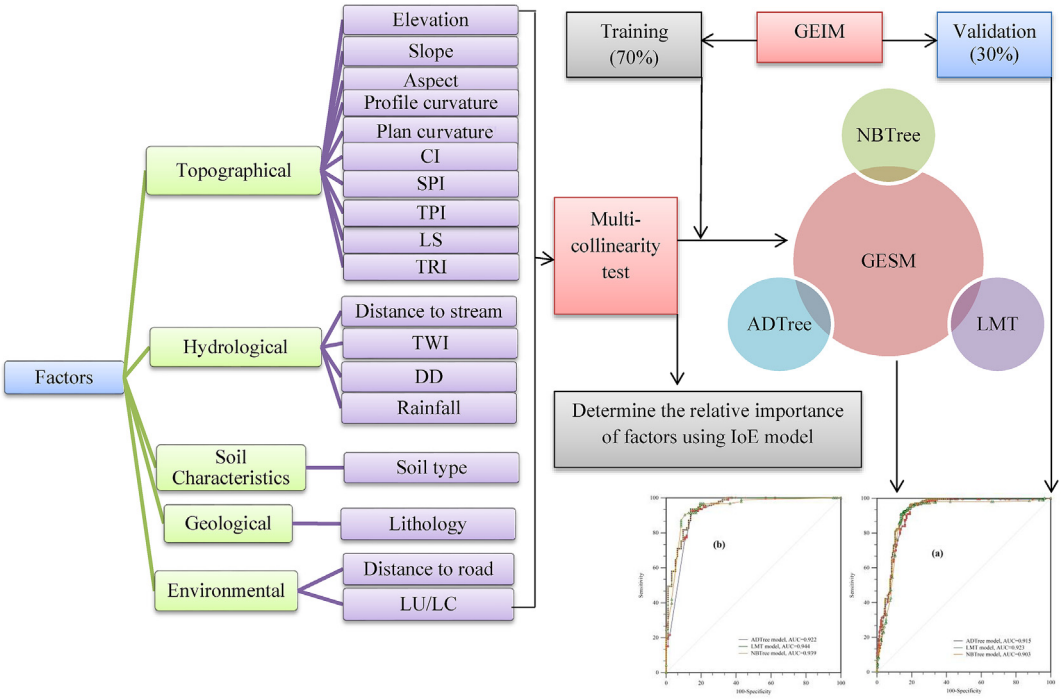

Fig. 3. Flowchart of research in the study area.

with rainfall and slope patterns they dictate overland flow propagation across the landscape. The Soil Type is also associated with a relative high weight (0.391). This may be linked to the soluble tendency of Aridisols and Entisols/Inceptisols types of soil. The former tends to show cracks which expand and contract as a function of soil moisture conditions. The latter is typically unconsolidated and thus, weak to water flux regimes which can detach and transport away soil particles. The IoE corresponds to the baseline information we use to interpret the local association between factors and gullies.

The overall weight obtained for the Elevation (0.383) suggests relatively stronger effect. And, the weights obtained for each separate class, indicate a greater estimated presence of gullies in the lowland. However, a very similar pattern can be seen in the Rainfall factor, where estimated gully occurrences are associated with lower precipitations. This could be a confounding effect between Elevation and Rainfall. These two properties are well known (Goovaerts, 2000) to be associated with one another (although our collinearity assessment did not detect it). And, a bivariate model is not suited with any routine that would deal with variable interaction. Therefore, it is not possible to understand whether the two factors convey a similar spatial effect over the final susceptibility map.

In terms of thematic influences to gully occurrences, the Lithology has a quite distinctive trait where seven out of ten lithotypes are not attributed with weights that suggest a relevant effect. Conversely, the complementary three classes have very high weights, which indicates a stronger association with the phenomena we modeled. Specifically, Group 6 (including Sandstone and Gypsiferous marl) reports a 1.19 wt which may be interpreted to be due to gully head-cuts established over soluble rock types. Group 8 still appears to positively contribute to gully presences, despite the relatively low weight (0.05). This group is highly variable, primarily featuring limestone alternated with shales, gypsiferous marl and conglomerates. The positive effect could be due to some localized presences of deposits rich in gypsum or because of the high mobility of conglomerates. Group 9 shows the highest relative weight, 2.24. This group generally includes deposits which are typical of a floodplain. As a result, the IoE may pick up the spatial signal where the gullies are actually located.

The NDVI ranges use here as proxies for the Land Use/Cover appear to contribute to gully erosion only within the moderate (IoE weight = 0.2) to poor (IoE weight = 2.58) classes. Such results suggest that prone conditions to gully can be found where local greenness is low, thus implying that bare or semi-bare soils may suffer from lack of protection from the vegetation cover. This is a quite reasonable interpretation and a patter that often arises in different erosion studies. For instance, Arabameri et al. (2018d) used the IoE and found that the highest weight corresponded to low-intermediate NDVI classes whereas the high NDVI showed an IoE weight equal to zero. This is also confirmed by Chaplot et al. (2005) where the authors clearly state that low greenness has a positive association with gully occurrence and development.

4.2. *Susceptibility mapping using three machine learning models*

Resulted maps using machine learning models are shown in Fig. 4a–c. As regard to the susceptibility mapping component, Table 4 reports how each of the three machine learning methods perform. The reported values correspond to the integrals of the Receiver Operating Characteristic curves (ROC) calculated for calibration (Success Rate Curve, SRC) and prediction (Prediction Rate Curve, PRC) (Lombardo and Mai, 2018).

The LMT appears to be outperforming the other two both in terms of SRC ($0.893 < 0.923 < 0.946$) and PRC ($0.900 < 0.944 < 0.972$) values, although the three models are producing outstanding results according to (Hosmer and Lemeshow, 2000). The standard error follows the same pattern being the minimum across the three models for the LMT, with SRC error equal to 0.0143 whereas for the PRC is 0.0160.

Looking at the corresponding ROC curves (see Fig. 5a and b), all the three models show similar pattern especially with respect to the False Positive Rates (or 100 - Specificity) within the first 20% bin up to True Positive Rates (Sensitivity) equal to 95% of the gully prone cases. The interesting finding shown here is that the same situation appears both for the calibration and validation subset. Even more surprisingly, the actual validation subset appears to be predicted with performances higher than the training set. This is quite uncommon, especially for Decision Trees which are known to produce overfit for within-sample models and lose much of those predictive abilities when predicting over out-of-sample cases (Schaffer, 1993).

Despite the uncommon results which may be due to the randomness of the sampling procedure, this relation suggests the original gully data

Table 3
Spatial relationship of gully locations and gully erosion conditioning factors.

Factor	Class	Percentage of gullies	Percentage of domain	IoE	
				FR	W
Slope (°)	<5	39.831	99.526	2.50	0.480
	5–10	10.105	0.474	0.05	
	10–15	8.405	0	0	
	15–20	9.740	0	0	
	20–30	19.014	0	0	
	>30	12.906	0	0	
Aspect	F	0.424	0.474	1.12	0.117
	N	8.957	5.213	0.58	
	NE	10.325	10.427	1.01	
	E	16.599	32.227	1.94	
	SE	23.090	33.175	1.44	
	S	18.541	16.114	0.87	
	SW	9.812	1.896	0.19	
	W	6.074	0	0	
	NW	6.179	0.474	0.08	
Elevation (m)	<1659	32.482	81.043	2.49	0.383
	1659–1990	20.964	18.957	0.90	
	1990–2342	16.238	0	0	
	2342–2724	14.156	0	0	
	2724–3163	9.946	0	0	
	>3163	6.214	0	0	
PC	Concave	38.715	49.289	1.27	0.107
	Flat	20.891	32.701	1.57	
	Convex	40.394	18.009	0.45	
Profile curvature	< −1.42	2.679	0	0	0.246
	−1.42 to −0.43	10.217	0	0	
	−0.43–0.28	66.858	95.261	1.42	
	0.28–1.27	16.924	4.739	0.28	
	>1.27	3.322	0	0	
CI	< −39.6	6.223	17.619	2.83	0.132
	−39.6 to −11.3	19.717	29.048	1.47	
	−11.3–9.01	45.125	32.381	0.72	
	9.01–38.03	23.238	14.762	0.64	
	>38.03	5.698	6.190	1.09	
LS (m)	<12.8	23.834	20.853	0.87	0.024
	12.8–31.2	14.937	11.374	0.76	
	31.2–50.6	13.375	9.953	0.74	
	50.6–69.5	14.316	21.327	1.49	
	69.5–87.02	18.932	25.118	1.33	
	>87.02	14.606	11.374	0.78	
TRI	<3.22	46.865	100	2.13	0.427
	3.22–7.43	19.410	0	0	
	7.43–11.64	19.325	0	0	
	11.64–17.59	11.838	0	0	
	>17.59	2.563	0	0	
TPI	< −10.74	4.679	0	0	0.309
	−10.74 to −3.3	15.803	0.474	0.03	
	−3.3–2.9	61.941	99.526	1.61	
	2.9 0 11.8	13.617	0	0	
	>11.8	3.960	0	0	
SPI	<9.16	21.839	39.336	1.80	0.105
	9.16–11.07	29.602	32.227	1.09	
	11.07–12.85	30.810	12.322	0.40	
	12.85–15.35	13.778	8.531	0.62	
	>15.35	3.970	7.583	1.91	
TWI	<4.86	39.432	0.474	0.01	0.373
	4.86–7.27	39.612	47.867	1.21	
	7.27–10.85	16.074	36.967	2.30	
	>10.85	4.883	14.692	3.01	
Dis to road (m)	<500	15.201	33.649	2.21	0.136
	500–1000	13.118	21.327	1.63	
	1000–1500	11.303	18.957	1.68	
	1500–2000	9.981	16.588	1.66	
	>2000	50.398	9.479	0.19	
Rainfall (mm)	<248.5	19.258	47.393	2.46	0.448
	248.5–350.3	36.240	52.133	1.44	
	350.3–461.02	21.764	0.474	0.02	
	461.02–582.7	14.082	0	0	
	>582.7	8.656	0	0	
Drainage density (km/km^2)	<0.85	26.957	0.939	0.03	0.565
	0.85–1.49	33.692	1.878	0.06	
	1.49–2.19	24.979	39.906	1.60	
	>2.19	14.372	57.277	3.99	
Dis to stream (m)	<100	27.675	45.024	1.63	0.130
	100–200	20.239	28.436	1.40	
	200–300	16.620	18.009	1.08	
	300–400	10.654	6.635	0.62	
	>400	24.811	1.896	0.08	
Lithology	Group 1	5.177	0	0	0.240
	Group 2	8.914	0	0	
	Group 3	7.768	0	0	
	Group 4	6.374	0	0	
	Group 5	2.283	0	0	
	Group 6	7.982	9.479	1.19	
	Group 7	2.137	0.000	0.00	
	Group 8	9.076	0.474	0.05	
	Group 9	40.248	90.047	2.24	
	Group 10	10.041	0	0	
LU/LC	Agriculture	19.034	31.754	1.67	0.248
	Dense-forest	0.010	0	0	
	Good-range	0.586	0	0	
	Agri-dryfarming	0.016	0	0	
	Dryfarming	1.099	0	0	
	Low-forest	22.846	0	0	
	Woodland	15.816	0	0	
	Mod-forest	5.655	0	0	
	Mod-range	7.148	1.422	0.20	
	Poor-range	25.868	66.825	2.58	
	Rock	1.567	0	0	
	Urban	0.353	0	0	
Soil type	Rock Outcrop/ Entisols	32.920	0.948	0.03	0.391
	Alfisols	0.480	0	0	
	Aridisols	10.935	3.318	0.30	
	Entisols/ Inceptisols	32.475	95.261	2.93	
	Inceptisols	1.677	0.474	0.28	
	Mollisols	21.513	0	0	

itself to exhibit low internal variability, irrespective of the sampling scheme. In turn, this allows us to consider the resulting susceptibility maps a reliable tool to predict gully erosion conditions over the study area. However, despite the high performances produced, the three susceptibility maps highlight quite significant differences where ADTree and LMT depict reasonable patterns although the NBTree essentially marks a binary condition, separating a large high-probability zone in the central area transitioning to a large low-probability zone with a very abrupt behavior. This is an important consideration because the dual scenario shown in the NBTree susceptibility has a poor geomorphological appearance. At times, many susceptibility studies focus on performance and disregard the fact that performances can be reached in very different ways, even non-realistic ways. For instance, Chen et al. (2017a) tested ADTree, NBTree and compared them to a Kernel Logistic Regression (KLR) model. Even in this study, they show very high performance but the fact that the KLR shows no low susceptibility values, even in flat regions, is not considered in depth. Another example can be found in Hosseinalizadeh et al. (2019b) where NBTree is shown to produce the highest performance among the considered tree-based methods although it essentially produces a near-binary predictive map.

To summarize such patterns in a numerical way, we computed the percentage of susceptibility classes distributed over the watershed. The results are shown in Fig. 6 where ADTree and LMT show a reasonable variation across the five susceptibility bins, however, as also pointed out above, NBTree almost classifies the watershed into very low (~68%) and very high (~30%) susceptibility conditions.

5. Discussions

Gully erosion susceptibility represents the first step to evaluate prone conditions to soil erosion. Therefore, it is also considered a proxy for

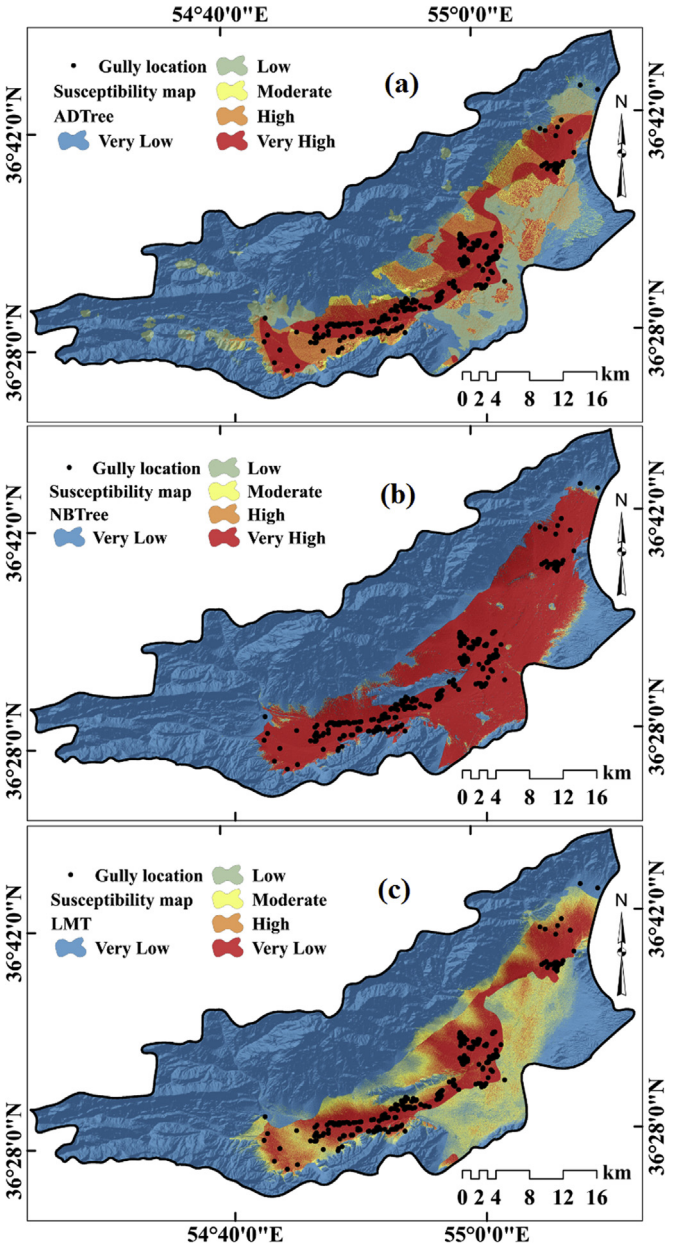

Fig. 4. Gully erosion susceptibility mapping.

hazard and risk assessment. Across the decision-making process, susceptibility models which offer high predictive performances are regarded as useful tools for governmental institutions, especially to develop gully erosion hazard prevention and mitigation strategies (Arabameri et al., 2019a). However, producing standardized and accurate gully erosion susceptibility maps at catchment or regional scales is not a straightforward task. In fact, accuracy can be determined via different metrics (Rahmati et al., 2019) and the number of algorithms is constantly increasing (Lombardo et al., 2016b) as technology improves computational efficiency. The latter represents one of the major challenges. Numerous modeling techniques have been proposed in the last decade to generate gully erosion susceptibility. And, finding an optimal method or workflow in comparative studies has been attempted by several gully erosion researchers (Conforti et al., 2011; Pourghasemi et al., 2017; Rahmati et al., 2017; Arabameri et al., 2019). This is the case for machine learning algorithms (Chen et al., 2017a). Such methods are constantly improved in other scientific branches and the geomorphological

Table 4
Values of validation results.

Method	Variable	AUC	SE	95% CI
SRC	ADTree	0.915	0.0147	0.884–0.940
	LMT	0.923	0.0143	0.893–0.946
	NBTree	0.903	0.0168	0.871–0.930
PRC	ADTree	0.922	0.0202	0.874–0.956
	LMT	0.944	0.0160	0.900–0.972
	NBTree	0.939	0.0177	0.894–0.969

community has invested a significant effort to keep up the technological pace, to test and to improve susceptibility models (Lombardo and Mai, 2018). In light of this broad scientific interest, here we investigated three methods namely Alternating Decision Tree, Naïve-Bayes tree and Logistic Model Tree machine learning model. In the current literature, such tests are rare and have yet to be tested in highly varying environmental conditions such as the arid to semi-arid territory of Iran.

We interpreted conditioning factors' effects by using Index of Entropy model. Drainage Density, Slope, and Rainfall appear to be the main drivers of the gullying process in the area together with soluble materials and low vegetation cover (Pourghasemi et al., 2012; Golestani et al., 2014; Arabameri et al., 2018d, 2019h). This combination suggests a primary hydrodynamic control on gully development which is a reasonable geomorphological explanation also supported by other studies in the neighboring catchments (Arabameri et al., 2018c).

A logical interpretation of these coexisting effects would assume that where gypsiferous marls outcrop without the protection of plants, the slope and drainage pattern in the area locally focus the impulsive rainfall discharges during the wet season and scour the landscape leaving the gully marks or developing those that already exist. This is a general interpretation that suits most of the watersheds located in the Northern regions in Iran. Several studies have produced similar conclusions (e.g., Arabameri et al., 2019a; Choubin et al., 2019), these being reached by using very different algorithms. As a result, one can infer that reaching similar conceptual models using different models neglects the randomness associated with single study cases. In turn, similar interpretations support a more generalized conceptual model for gully erosion prediction within the whole Semnan province. Therefore, from the territorial management standpoint, we can suggest conservation practices to better manage/control overland flows resulting from concentrated rainfall.

With regard to the predictive mapping component of this contribution, the three algorithms did not converge to a common outcome. In fact, NBTree essentially classifies the area into two classes (see Fig. 4b) without providing a more continuous distinction in probabilistic terms. This is probably due to a model convergence issue where the NBTree gets a satisfactory differentiation between gully/no-gully conditions via a very simplified rule. As a consequence, the depth of the tree stops at the combination of few parameters, and does not draw strength from the variability associated with other conditioning factors. Conversely, ADTree and LMT provide a much more spread and realistic distribution in the probability estimates, although the latter model is able to produce even better performance. The spatial realization of the two models is similar at a catchment scale. However, a careful observation of the susceptibility patterns shows that the ADTree returns probability classes distributed over very discrete spatial bins. In other words, the susceptibility maps alternates spatial clusters of homogenous probability estimates and the passage between clusters is quite abrupt (see Fig. 4a). This is clearly not the case for the LMT where a more natural distribution of susceptibility patterns is reported in Fig. 4c. One could argue that the discrete transition shown by the ADTree is logically linked to the soluble outcrops, thus being a reasonable spatial trend. However, similar to the interpretation mentioned above for the NBTree, we believe it to be an evidence of a decision tree which did not grow in depth, therefore exploiting the whole information conveyed by other properties/

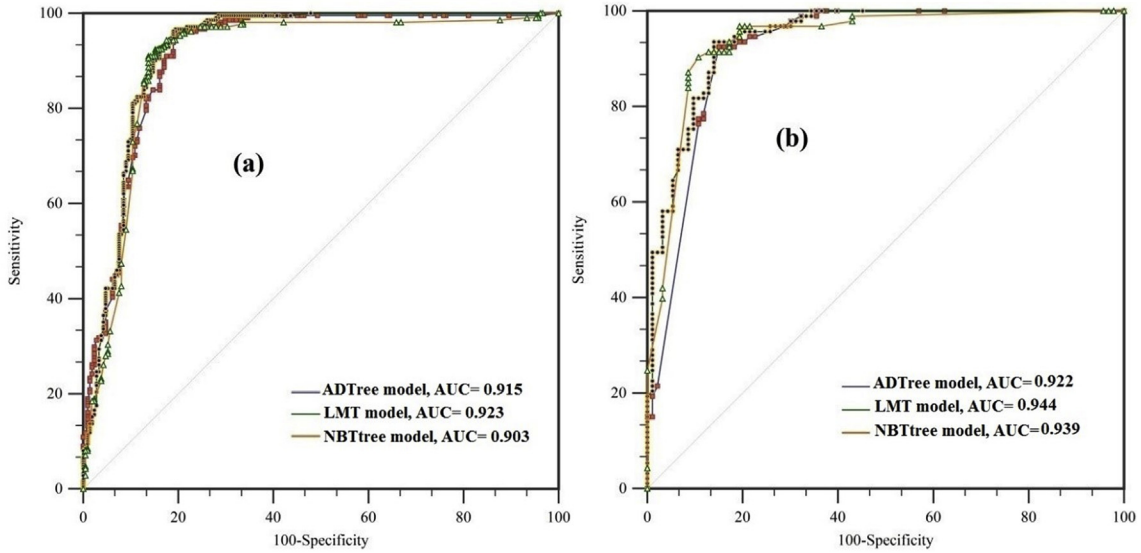

Fig. 5. Area under the curve. (a) Training dataset (success rate curve), (b) validation dataset (prediction rate curve).

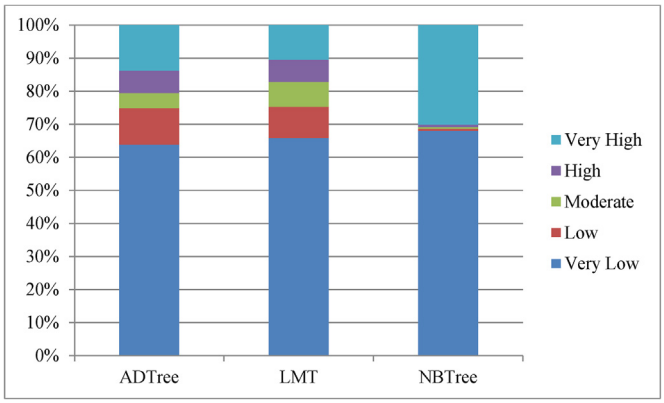

Fig. 6. Percentage of susceptibility classes in different models.

conditioning factors. On the contrary, the appearance of the LMT-based susceptibility maps depicts a much smoother process, where gully erosion conditions transition from one area to the other in a continuous form where the signal coming from the main predictors is stacked together with the signal originated by minor but still relevant conditioning factors. This is certainly the case for the moderate susceptibility class in the LMT model located to the south. The same class is shown to be associated with low susceptibility conditions for the ADTree and with very high conditions for the NBTree. This region corresponds to areas with moderate range vegetation (see class K in Land Use/Cover in Fig. 2) and it marks a clear lack of the NBTree and ADTree in capturing the associated effect in the model. This is something that we have found also in other articles, where methods that appear to be highly skilled in predicting gully occurrences produce unnatural susceptibility patterns. For instance, Chen et al. (2017a) show a map produced via KLR where there is no sign of non-susceptible areas despite other methods the authors tested clearly show low probability zones. Similarly, Hosseinalizadeh et al. (2019b) show the same issue we have found with the NBTree. The resulting gully erosion susceptibility map is almost binary despite other tested methods producing a much broader distribution of probability values. We stressed this concept because oftentimes the only metric used to describe performance in gully erosion susceptibility is the AUC. However, we believe that a much broader spectrum of metrics should be evaluated and among them, the geomorphological sense of the susceptibility map.

We recall that the dataset fed to the three model is identical and differences are uniquely due to the different algorithmic structure. Therefore, we consider LMT a much more suitable method to map gully-prone conditions. Overall, the combination of remote sensing, GIS and data mining tools offer high accuracy for gully erosion predictions and lead to gully erosion susceptibility maps which could assist decision-makers for environmental management. Such maps could also be accepted as proxies for gully erosion risk management studies, supporting territorial management practices as a whole.

6. Conclusion

We modeled gully erosion susceptibility conditions in the Bastam watershed, which is known to suffer from widespread gullying processes. In fact, local communities are already affected by soil removal which not only threatens agricultural practices but also local infrastructure in the form of road network and electric powerlines. In this work, we built three separate susceptibility models whose differences are only imputable to the algorithmic differences among NBTree, ADTree and LMT. These are three variations of decision trees whose usage extends over different scientific applications. The results in this paper indicate similar performances among the three employed algorithms. However, pure performance metrics cannot be the only parameter to interpret the reliability of a given susceptibility estimation. In fact, although negligible differences are shown in terms of raw AUC values, a much more interesting variation affects the actual predictive maps. The NBTree depicts a non-informative binary situation where very high probability values characterize the central sector of the Bastam watershed. However, building a susceptibility map is meant to support decision-making processes. For instance, on the basis of a susceptibility trend in space, local administrations should prioritize investments or raise awareness in the local communities. And, by examining the NBTree-based gully erosion susceptibility map, the resulting pattern is a non-differentiable blur which provide little to no useful information. A much better situation is shown in the ADTree-based map, although the growth of the associated tree is still not sufficient, especially when compared to the output coming from the LMT model. The latter not only outperforms the other methods but produces much more natural susceptibility patterns in space, making it a credible tool to understand areas where future gullies may initiate and develop over time. This information can be easily incorporated in a much larger scientific effort that Iranian institutions are currently focused on to understand, isolate and limit soil erosion across the whole country. The LMT model was trained using freely-accessible information both on

gullies' distribution and conditioning factors. In addition, it does not require powerful computing facilities, which makes it an appealing tool to assess any environmental hazards. Ultimately, one of the main weaknesses of machine learning algorithms consists of a limited ability to produce quantitative estimates of conditioning factors' effects. In fact, no interpretable regression coefficients nor weights are provided, which is otherwise a native output of statistical models, although the latter do not produce equally satisfying predictive performance. We bypassed this difference by interpreting environmental predisposing conditions on the basis of a simple and straightforward bivariate statistical model namely, Index of Entropy. This tool was able to highlight associations between conditioning factors and gully occurrences returning quantitative weights which supported not only our interpretation but also the patterns arose from the susceptibility estimates. Similar to the considerations mentioned above, the IoE can be integrated in any susceptibility study for its simplicity allows computing weights quite rapidly and without significant computational requirements.

Declaration of competing interest

The authors declare that they have no known competing financial interests or personal relationships that could have appeared to influence the work reported in this paper.

References

Akgün, A., Türk, N., 2011. Mapping erosion susceptibility by a multivariate statistical method: a case study from the Ayvalk region, NW Turkey. Comput. Geosci. 37 (9), 1515–1524.

Amundson, R., Berhe, A.A., Hopmans, J.W., Olson, C., Sztein, A.E., Sparks, D.L., 2015. Soil and human security in the 21st century. Science 348 (6235), 1261071.

Arabameri, A., Pradhan, B., Pourghasemi, H., Rezaei, K., Kerle, N., 2018a. Spatial modelling of gully erosion using GIS and R programing: a comparison among three data mining algorithms. Appl. Sci. 8 (8), 1369.

Arabameri, A., Pradhan, B., Pourghasemi, H.R., Rezaei, K., 2018b. Identification of erosion-prone areas using different multi-criteria decision-making techniques and GIS. Geomatics, Nat. Hazards Risk 9 (1), 1129–1155.

Arabameri, A., Pradhan, B., Rezaei, K., Yamani, M., Pourghasemi, H.R., Lombardo, L., 2018c. Spatial modelling of gully erosion using evidential belief function, logistic regression, and a new ensemble of evidential belief function–logistic regression algorithm. Land Degrad. Dev. 29 (11), 4035–4049.

Arabameri, A., Rezaei, K., Pourghasemi, H.R., Lee, S., Yamani, M., 2018d. GIS-based gully erosion susceptibility mapping: a comparison among three data-driven models and AHP knowledge-based technique. Environmental earth sciences 77 (17), 628.

Arabameri, A., Pradhan, B., Rezaei, K., 2019a. Gully erosion zonation mapping using integrated geographically weighted regression with certainty factor and random forest models in GIS. J. Environ. Manag. 232, 928–942.

Arabameri, A., Pradhan, B., Rezaei, K., 2019b. Spatial prediction of gully erosion using ALOS PALSAR data and ensemble bivariate and data mining models. Geosci. J. 1–18.

Arabameri, A., Pradhan, B., Rezaei, K., Conoscenti, C., 2019c. Gully erosion susceptibility mapping using GIS-based multi-criteria decision analysis techniques. Catena 180, 282–297.

Arabameri, A., Pradhan, B., Rezaei, K., Lee, C.-W., 2019d. Assessment of landslide susceptibility using statistical-and artificial intelligence-based FR–RF integrated model and multiresolution DEMs. Remote Sens. 11 (9), 999.

Arabameri, A., Pradhan, B., Rezaei, K., Sohrabi, M., Kalantari, Z., 2019e. GIS-based landslide susceptibility mapping using numerical risk factor bivariate model and its ensemble with linear multivariate regression and boosted regression tree algorithms. J. Mt. Sci. 16 (3), 595–618.

Arabameri, A., Rezaei, K., Cerdà, A., Conoscenti, C., Kalantari, Z., 2019f. A comparison of statistical methods and multi-criteria decision making to map flood hazard susceptibility in Northern Iran. Sci. Total Environ. 660, 443–458.

Arabameri, A., Rezaei, K., Cerda, A., Lombardo, L., Rodrigo-Comino, J., 2019g. GIS-based groundwater potential mapping in Shahroud plain, Iran. A comparison among statistical (bivariate and multivariate), data mining and MCDM approaches. Sci. Total Environ. 658, 160–177.

Arabameri, A., Cerda, A., Tiefenbacher, J.P., 2019h. Spatial pattern analysis and prediction of gully erosion using novel hybrid model of entropy-weight of evidence. Water 11 (6), 1129.

Arabameri, A., Pradhan, B., Lombardo, L., 2019i. Comparative assessment using boosted regression trees, binary logistic regression, frequency ratio and numerical risk factor for gully erosion susceptibility modelling. CATENA 2019 183, 104223.

Arabameri, A., Yamani, M., Pradhan, B., Melesse, A., Shirani, K., Tien Bui, D., 2019j. Novel ensembles of COPRAS multi-criteria decision-making with logistic regression, boosted regression tree, and random forest for spatial prediction of gully erosion susceptibility. Sci. Total Environ. 688, 903–916.

Beven, K.J., Kirkby, M.J., 1979. A physically based, variable contributing area model of basin hydrology/Un modèle à base physique de zone d'appel variable de l'hydrologie du bassin versant. Hydrol. Sci. J. 24 (1), 43–69.

Bout, B., Lombardo, L., Westen, C.J.V., Jetten, V.G., 2018. Integration of two-phase solid fluid equations in a catchment model for flashfloods, debris flows and shallow slope failures. Environ. Model. Softw 105, 1–16.

Cama, M., Lombardo, L., Conoscenti, C., Rotigliano, E., 2017. Improving transferability strategies for debris flow susceptibility assessment: application to the Saponara and Itala catchments (Messina, Italy). Geomorphology 288, 52–65.

Camilo, D.C., Lombardo, L., Mai, P.M., Jie, D., Huser, R., 2017. Handling high predictor dimensionality in slope-unit-based landslide susceptibility models through LASSO-penalized Generalized Linear Model. Environ. Model. Softw 97, 145–156.

Capra, A., Ferro, V., Porto, P., Scicolone, B., 2012. Quantifying interrill and ephemeral gully erosion in a small Sicilian basin interrill and ephemeral gully erosion in a small Sicilian basin. Z. Geomorphol. 56 (1), 9–25.

Cartagena, D.F., 2004. Remotely Sensed Land Cover Parameter Extraction for Watershed Erosion Modelling. ITC, pp. 1–104.

Chaplot, V., Coadou le Brozec, E., Silvera, N., Valentin, C., 2005. Spatial and temporal assessment of linear erosion in catchments under sloping lands of northern Laos. Catena 63, 167–184.

Chen, W., Shirzadi, A., Shahabi, H., Ahmad, B.B., Zhang, S., Hong, H., Zhang, N., 2017a. A novel hybrid artificial intelligence approach based on the rotation forest ensemble and naïve Bayes tree classifiers for a landslide susceptibility assessment in Langao County, China. Geomatics, Nat. Hazards Risk 8 (2), 1955–1977.

Chen, W., Xie, X., Peng, J., Wang, J., Duan, Z., Hong, H., 2017b. GIS-based landslide susceptibility modelling: a comparative assessment of kernel logistic regression, Naïve-Bayes tree, and alternating decision tree models. Geomatics, Nat. Hazards Risk 8 (2), 950–973.

Chen, W., Pradhan, B., Li, S., Shahabi, H., Rizeei, H.M., Hou, E., Wang, S., 2019. Novel hybrid integration approach of bagging-based Fisher's linear discriminant function for groundwater potential analysis. Nat. Resour. Res. 1–20.

Choubin, B., Rahmati, O., Tahmasebipour, N., Feizizadeh, B., Pourghasemi, H.R., 2019. Application of fuzzy analytical network process model for analyzing the gully erosion susceptibility. In: Natural Hazards GIS-Based Spatial Modeling Using Data Mining Techniques. Springer, Cham, pp. 105–125.

Claps, P., Fiorentino, M., Oliveto, G., 1994. Informational entropy of fractal river networks. J. Hydrol. 187 (1–2), 145–156.

Conforti, M., Aucelli, P.P.C., Robustelli, G., Scarciglia, F., 2011. Geomorphology and GIS analysis for mapping gully erosion susceptibility in the Turbolo stream catchment (Northern Calabria, Italy). Nat. Hazards 56 (3), 881–898.

Daba, S., Rieger, W., Strauss, P., 2003. Assessment of gully erosion in eastern Ethiopia using photogrammetric techniques. Catena 50 (2–4), 273–291.

Dazzi, C., Cornelis, W., Costantini, E.A., Dumitru, M., Fullen, M.A., Gabriels, D., Kasparinskis, R., Kertész, A., Papa, G.L., Pérès, G., 2019. The contribution of the European Society for Soil Conservation (ESSC) to scientific knowledge, education and sustainability. International Soil and Water Conservation Research 7 (1), 102–107.

Desmet, P., Govers, G., 1996. A GIS procedure for automatically calculating the USLE LS factor on topographically complex landscape units. J. Soil Water Conserv. 51 (5), 427–433.

Dietterich, T., 1995. Overfitting and undercomputing in machine learning. ACM Comput. Surv. 27 (3), 326–327.

Freund, Y., Mason, L., 1999. The Alternating Decision Tree Learning Algorithm. In: Proceeding of the International Conference on Machine Learning.

Gholami, V., 2013. The influence of deforestation on runoff generation and soil erosion (Case study: kasilian Watershed). J. For. Sci. 59 (7), 272–278.

Ghorbani Nejad, S., Falah, F., Daneshfar, M., Haghizadeh, A., Rahmati, O., 2016. Delineation of groundwater potential zones using remote sensing and GIS-based data-driven models. Geocarto Int. 32, 167–187.

Golestani, G., Issazadeh, L., Serajamani, R., 2014. Lithology effects on gully erosion in Ghoori chay Watershed using RS & GIS. Int. J. Biosci. 4, 71–76.

Goovaerts, P., 2000. Geostatistical approaches for incorporating elevation into the spatial interpolation of rainfall. J. Hydrol. 228 (1), 113–129.

GSI, 1997. Geology survey of Iran. http://www.gsi.ir/Main/Lang_en/index.html.

Gutiérrez, Á.G., Schnabel, S., Felicísimo, Á.M., 2010. Modelling the occurrence of gullies in rangelands of southwest Spain. Earth Surf. Process. Landforms 34 (14), 1894–1902.

Heerdegen, R.G., Beran, M.A., 1982. Quantifying source areas through land surface curvature and shape. J. Hydrol. 57 (3), 359–373.

Herrick, J., Weltz, M., Schuman, G., Reeder, J., Simanton, J., 2019. Rangeland soil erosion and soil quality: Role of soil resistance, resilience, and disturbance regime. In: Soil Quality and Soil Erosion. CRC Press, pp. 209–233. https://doi.org/10.1201/9780203739266-13.

Hosmer, D.W., Lemeshow, S., 2000. Applied Logistic Regression. John Wiley & Sons, New York.

Hosseinalizadeh, M., Kariminejad, N., Rahmati, O., Keesstra, S., Alinejad, M., Behbahani, A.M., 2019a. How can statistical and artificial intelligence approaches predict piping erosion susceptibility? Sci. Total Environ. 646, 1554–1566.

Hosseinalizadeh, M., Kariminejad, N., Chen, W., Pourghasemi, H.R., Alinejad, M., Behbahani, A.M., Tiefenbacher, J.P., 2019b. Gully headcut susceptibility modeling using functional trees, naïve Bayes tree, and random forest models. Geoderma 342, 1–11.

Huang, J., Lu, J., Ling, C.X., 2003. Comparing naive Bayes, decision trees, and SVM with AUC and accuracy. In: Third IEEE International Conference on Data Mining. IEEE, pp. 553–556.

Imwangana, F.M., Dewitte, O., Ntombi, M., Moeyersons, J., 2014. Topographic and road control of mega-gullies in Kinshasa (DR Congo). Geomorphology 217, 131–139.
IRIMO, 2012. In: Summary Reports of Iran's Extreme Climatic Events. Ministry of roads and urban development, Iran Meteorological Organization. www.cri.ac.ir.
Jaafari, A., Najafi, A., Pourghasemi, H., Rezaeian, J., Sattarian, A., 2014. GIS-based frequency ratio and index of entropy models for landslide susceptibility assessment in the Caspian forest, northern Iran. Int. J. Environ. Sci. Technol. 11 (4), 909–926.
Kadavi, P.R., Lee, C.-W., Lee, S., 2019. Landslide-susceptibility mapping in Gangwon-do, South Korea, using logistic regression and decision tree models. Environmental Earth Sciences 78 (4), 116.
Kelava, A., Moosbrugger, H., Dimitruk, P., Schermelleh-Engel, K., 2008. Multicollinearity and missing constraints: a comparison of three approaches for the analysis of latent nonlinear effects. Methodology 4 (2), 51–66.
Kheir, R.B., Wilson, J., Deng, Y., 2007. Use of terrain variables for mapping gully erosion susceptibility in Lebanon. Earth Surf. Process. Landforms (12), 1770–1782.
Kheir, R.B., Chorowicz, J., Abdallah, C., Dhont, D., 2008. Soil and bedrock distribution estimated from gully form and frequency: a GIS-based decision-tree model for Lebanon. Geomorphology 93 (3–4), 482–492.
Kropacek, J., Schillaci, C., Salvini, R., Marker, M., 2016. Assessment of gully erosion in the Upper Awash, Central Ethiopian highlands based on a comparison of archived aerial photographs and very high resolution satellite images. Geogr. Fis. Din. Quaternaria 39 (2), 161–170.
Kümmerer, K., Held, M., Pimentel, D., 2010. Sustainable use of soils and time. J. Soil Water Conserv. 65 (2), 141–149.
LANDWEHR, N., Hall, M., Frank, E., 2003. Logistic model trees. In: European Conference on Machine Learning. Springer, pp. 241–252.
Lombardo, L., Mai, P.M., 2018. Presenting logistic regression-based landslide susceptibility results. Eng. Geol. 244, 14–24.
Lombardo, L., Cama, M., Maerker, M., Rotigliano, E., 2014. A test of transferability for landslides susceptibility models under extreme climatic events: application to the Messina 2009 disaster. Nat. Hazards 74 (3), 1951–1989.
Lombardo, L., Cama, M., Conoscenti, C., Märker, M., Rotigliano, E., 2015. Binary logistic regression versus stochastic gradient boosted decision trees in assessing landslide susceptibility for multiple-occurring landslide events: application to the 2009 storm event in Messina (Sicily, southern Italy). Nat. Hazards 79 (3), 1621–1648.
Lombardo, L., Bachofer, F., Cama, M., Märker, M., Rotigliano, E., 2016a. Exploiting Maximum Entropy method and ASTER data for assessing debris flow and debris slide susceptibility for the Giampilieri catchment (north-eastern Sicily, Italy). Earth Surf. Process. Landforms 41 (12), 1776–1789.
Lombardo, L., Fubelli, G., Amato, G., Bonasera, M., 2016b. Presence-only approach to assess landslide triggering-thickness susceptibility: a test for the Mili catchment (north-eastern Sicily, Italy). Nat. Hazards 84 (1), 565–588.
Lombardo, L., Opitz, T., Huser, R., 2019a. Numerical recipes for landslide spatial prediction using R-INLA: a step-by-step tutorial. In: Spatial Modeling in GIS and R for Earth and Environmental Sciences. Elsevier, pp. 55–83.
Lombardo, L., Bakka, H., Tanyas, H., van Westen, C., Mai, P.M., Huser, R., 2019b. Geostatistical modeling to capture seismic-shaking patterns from earthquake-induced landslides. J. Geophys. Res.: Earth Surface 124, 1958–1980.
Lucà, F., Conforti, M., Robustelli, G., 2011. Comparison of GIS-based gullying susceptibility mapping using bivariate and multivariate statistics: northern Calabria, South Italy. Geomorphology 134 (3–4), 297–308.
Magliulo, P., 2012. Assessing the susceptibility to water-induced soil erosion using a geomorphological, bivariate statistics-based approach. Environ. Earth Sci. 67 (6), 1801–1820.
Mandrekar, J.N., 2010. Receiver operating characteristic curve in diagnostic test assessment. J. Thorac. Oncol. 5 (9), 1315–1316.
Montgomery, D.R., Dietrich, W.E., 1992. Channel initiation and the problem of landscape scale. Science 255, 826.
Moore, I.D., Grayson, R.B., 1991. Terrain-based catchment partitioning and runoff prediction using vector elevation data. Water Resour. Res. 27 (6), 1177–1191.
Nefeslioglu, H.A., Gokceoglu, C., Sonmez, H., 2008. An assessment on the use of logistic regression and artificial neural networks with different sampling strategies for the preparation of landslide susceptibility maps. Eng. Geol. 97 (3–4), 171–191.
Niipele, J.N., Chen, J., 2019. The usefulness of alos-palsar dem data for drainage extraction in semi-arid environments in the Iishana sub-basin. J. Hydrol.: Reg. Stud. 21, 57–67.
Olaya, V., Conrad, O., 2009. Geomorphometry in SAGA. Dev. Soil Sci. 33, 293–308.
Panagos, P., Borrelli, P., Poesen, J., Ballabio, C., Lugato, E., Meusburger, K., Montanarella, L., Alewell, C., 2015. The new assessment of soil loss by water erosion in Europe. Environ. Sci. Policy 54, 438–447.
Parras-Alcántara, L., Lozano-García, B., Keesstra, S., Cerdà, A., Brevik, E.C., 2016. Long-term effects of soil management on ecosystem services and soil loss estimation in olive grove top soils. Sci. Total Environ. 571, 498–506.
Pham, B.T., Bui, D.T., Prakash, I., 2017. Landslide susceptibility assessment using bagging ensemble based alternating decision trees, logistic regression and J48 decision trees methods: a comparative study. Geotech. Geol. Eng. 35 (6), 2597–2611.
Pimentel, D., Burgess, M., 2013. Soil erosion threatens food production. Agriculture 3 (3), 443–463.
Poesen, J., Vandaele, K., van Wesemael, B., 1998. Gully erosion: importance and model implications. In: Boardman, J., Favis-Mortlock, D. (Eds.), Modelling Soil Erosion by Water. Springer, Berlin, pp. 285–311.
Pourghasemi, H.R., Rossi, M., 2017. Landslide susceptibility modeling in a landslide prone area in Mazandarn Province, north of Iran: a comparison between GLM, GAM, MARS, and M-AHP methods. Theor. Appl. Climatol. 130 (1–2), 609–633.
Pourghasemi, H.R., Mohammady, M., Pradhan, B., 2012. Landslide susceptibility mapping using index of entropy and conditional probability models in GIS: safarood Basin, Iran. Catena 97, 71–84.
Pourghasemi, H.R., Yousefi, S., Kornejady, A., Cerdà, A., 2017. Performance assessment of individual and ensemble data-mining techniques for gully erosion modeling. Sci. Total Environ. 609, 764–775.
Rahmati, O., Haghizadeh, A., Pourghasemi, H.R., Noormohamadi, F., 2016. Gully erosion susceptibility mapping: the role of GIS-based bivariate statistical models and their comparison. Nat. Hazards 82 (2), 1231–1258.
Rahmati, O., Tahmasebipour, N., Haghizadeh, A., Pourghasemi, H.R., Feizizadeh, B., 2017. Evaluation of different machine learning models for predicting and mapping the susceptibility of gully erosion. Geomorphology 298, 118–137.
Rahmati, O., Kornejady, A., Samadi, M., Deo, R.C., Conoscenti, C., Lombardo, L., Dayal, K., Taghizadeh-Mehrjardi, R., Pourghasemi, H.R., Kumar, S., 2019. PMT: new analytical framework for automated evaluation of geo-environmental modelling approaches. Sci. Total Environ. 664, 296–311.
REFAHI, H., 2009. Soil erosion by water & amp; conservation. In: Farsi with English Summary. Tehran University Press, pp. 10–202.
Reu, J.D., Bourgeois, J., Bats, M., Zwertvaegher, A., Gelorini, V., Smedt, P.D., Wei, C., Antrop, M., Maeyer, P.D., Finke, P., 2013. Application of the topographic position index to heterogeneous landscapes. Geomorphology 186 (15), 39–49.
Roux, H., Labat, D., Garambois, P.-A., Maubourguet, M.-M., Chorda, J., Dartus, D., 2011. A physically-based parsimonious hydrological model for flash floods in Mediterranean catchments. Nat. Hazards Earth Syst. Sci. 11 (9), 2567–2582.
Samani, A.N., Ahmadi, H., Jafari, M., Boggs, G., Ghoddousi, J., Malekian, A., 2009. Geomorphic threshold conditions for gully erosion in Southwestern Iran (Boushehr-Samal watershed). J. Asian Earth Sci. 35 (2), 180–189.
Schaffer, C., 1993. Overfitting avoidance as bias. Mach. Learn. 10 (2), 153–178.
Skidmore, E., 1982. Wind erosion control. Cli. Change 9, 209–218. https://doi.org/10.1007/BF00140537.
Sok, H.K., Ooi, M.P.-L., Kuang, Y.C., Demidenko, S., 2016. Multivariate alternating decision trees. Pattern Recognit. 50, 195–209.
Takken, I., Croke, J., Lane, P., 2008. Thresholds for channel initiation at road drain outlets. Catena 75 (3), 257–267.
Tien Bui, D., Pradhan, B., Lofman, O., Revhaug, I., 2012. Landslide susceptibility assessment in Vietnam using support vector machines, decision tree, and Naive Bayes Models. Math. Probl. Eng. 2012, 974638 https://doi.org/10.1155/2012/974638.
Tien Bui, D., Ho, T.-C., Pradhan, B., Pham, B.-T., Nhu, V.-H., Revhaug, I., 2016. GIS-based modeling of rainfall-induced landslides using data mining-based functional trees classifier with AdaBoost, Bagging, and MultiBoost ensemble frameworks. Environmental Earth Sciences 75 (14), 1101.
Trigila, A., Iadanza, C., Esposito, C., Scarascia-Mugnozza, G., 2015. Comparison of logistic regression and random forests techniques for shallow landslide susceptibility assessment in Giampilieri (NE sicily, Italy). Geomorphology 249, 119–136.
Wang, S., Jiang, L., Li, C., 2015. Adapting naive Bayes tree for text classification. Knowl. Inf. Syst. 44 (1), 77–89.
Wang, L.-J., Guo, M., Sawada, K., Lin, J., Zhang, J., 2016. A comparative study of landslide susceptibility maps using logistic regression, frequency ratio, decision tree, weights of evidence and artificial neural network. Geosci. J. 20 (1), 117–136.
Xiong, M., Sun, R., Chen, L., 2018. Effects of soil conservation techniques on water erosion control: a global analysis. Sci. Total Environ. 645, 753–760.
Zabihi, M., Mirchooli, F., Motevalli, A., Darvishan, A.K., Pourghasemi, H.R., Zakeri, M.A., Sadighi, F., 2018. Spatial modelling of gully erosion in Mazandaran Province, northern Iran. Catena 161, 1–13.
Zakerinejad, R., Maerker, M., 2015. An integrated assessment of soil erosion dynamics with special emphasis on gully erosion in the Mazayjan basin, southwestern Iran. Nat. Hazards 79, S25–S50.
Zevenbergen, L.W., Thorne, C.R., 1987. Quantitative analysis of land surface topography. Earth Surf. Process. Landforms 12 (1), 47–56.
Zhao, L., Hou, R., 2019. Human causes of soil loss in rural karst environments: a case study of Guizhou, China. Sci. Rep. 9 (1), 3225.